Journal of Photochemistry & Photobiology A: Chemistry 367 (2018) 365–374

Contents lists available at ScienceDirect

Journal of Photochemistry & Photobiology A: Chemistry

journal homepage: www.elsevier.com/locate/jphotochem

Photodissociation of trifluoroacetic acid at 193 nm: Mechanism for formation of OH radical and stable products

Sumana SenGupta*, Ankur Saha, Awadhesh Kumar*,[1], Prakash D. Naik[1]

Radiation & Photochemistry Division, Bhabha Atomic Research Centre, Mumbai, 400 085, India

ARTICLE INFO

Keywords:
Trifluoroacetic acid
Photodissociation
OH radical
Dynamics
Laser Induced Fluorescence

ABSTRACT

Trifluoroacetic acid (TFA) is released in the atmosphere through its use in the chemical industry and as degradation product of chlorofluorocarbon (CFC) alternatives like hydrofluorocarbons and hydrochlorofluorocarbons. In the present study, we have investigated the OH formation dynamics in the photodissociation of TFA at 193 nm by Laser Photolysis-Laser Induced Fluorescence (LP-LIF) method, as well as stable product formation by GC–MS and FTIR. It was found that, ~26% of the available energy is partitioned into the relative translation of the photoproducts ($f(T) = 0.26$), which could be explained by presence of an exit barrier of ~13 kcal/mol in OH formation channel. This result is very similar to OH formation from acetic acid (AA) and difluoroacetic acid (DFA), indicating fluorination at the side chain of aliphatic carboxylic acids does not significantly change the mechanism of C–OH bond scission. Our experimental results tallied with the theoretical studies, which suggested that the major OH formation channel in acetic acid and fluoroacetic acid is direct dissociation from the optically excited S_1 state through an exit barrier, with some competition from the T_1 state. However, quantum yield of OH formation from TFA (0.4) was found to be much smaller than AA (0.8), which is probably caused by higher reaction barrier in T_1 state of TFA, compared to AA. CHF_3, C_2F_4, C_2F_6, CO_2, CO, CF_3CFO, CF_2O and hexafluoropropylene oxide (HFPO) were detected as the stable products of the photolysis of TFA. The theoretically optimized ground state dissociation channels showed significant difference between TFA and AA.

1. Introduction

Trifluoroacetic acid (TFA) is commonly used in the chemical industry as synthetic as well as analytical reagent [1,2]. It has also been identified as the end product of the atmospheric degradation of hydrochlorofluorocarbons (HCFCs), hydrofluorocarbons (HFCs), and long chain poly fluorinated compounds (PFCs) which are used as CFC alternatives [3–5]. A very small contribution to the environmental TFA can also come from the biological or atmospheric oxidation of anesthetics like halothane and isoflurane [6,7]. To assess the environmental impact of TFA and other fluorinated carboxylic acids, their gas-phase dissociation has been extensively investigated [8–16]. The dissociation of TFA, by different methods like thermolysis [8–10], pyrolysis [11], IRMPD [12] and photodissociation [13,9–16] is already reported. It is also been established that, decarboxylation and dehydration are the major photodissociation channels at lower wavelengths (190–220 nm) [17,18] for acetic acid (AA), but not in case of difluoroacetic acid (DFA). Rather, γ-elimination of hydrogen fluoride was found to be the most important channel in thermal decomposition, IRMPD and UV laser photolysis of DFA [9,16]. But the dynamics for OH formation by photodissociation at 193–220 nm, is reported to be similar in case of carboxylic acids [17–20], and fluoroacetic acids [13–15,21]. For both fluorinated and non-fluorinated carboxylic acids, earlier, it was proposed that the initially populated S_1 state undergoes radiationless transition to a nearby triplet state, and the OH generation channel takes place from both the triplet and singlet states, the former being more dominant. Accordingly, in the previously reported comparison between the OH formation from photodissociation of TFA and AA at 193 nm, the results were discussed assuming that major channel operates predominantly from the T_1 state, with some contribution from the S_1 state [14]. However, in the more recent theoretical studies [17,22], it was found that in case of fluorinated carboxylic acids, OH formation from the S_1 state itself is one of the major channels.

Since the current theoretical studies predict the mechanism to be quite different, it is important to re-evaluate the dynamics of OH formation from TFA. In order to understand the actual nature of the

* Corresponding authors.
E-mail addresses: [redacted]@barc.gov.in (S. SenGupta), [redacted]@barc.gov.in (A. Kumar).
[1] Also affiliated to Homi Bhabha National Institute, Anushaktinagar, 400 094, Mumbai, India.

https://doi.org/10.1016/j.jphotochem.2018.08.039
Received 7 June 2018; Received in revised form 21 August 2018; Accepted 25 August 2018
Available online 03 September 2018

potential energy surface for dissociation, we have investigated the OH formation dynamics, as well as stable product formation in the photodissociation of TFA by 193 nm laser. To form a comprehensive idea about the dissociation mechanism, we have compared our results with the current theoretical studies in details. To determine the actual effect of fluorination on the photodissociation mechanism of carboxylic acids, the results were also extensively compared with that of AA and DFA. Theoretical calculations for dissociation from both the ground state and the excited states were discussed to support our experimental results.

2. Method and methodologies

2.1. Experimental

Trifluoroacetic acid (> 99.0% purity) was procured from Sigma Aldrich and used after repeated freeze-pump-thaw cycles. Its dissociation was studied using the Laser Photolysis–Laser Induced Fluorescence technique. The experimental set-up is same as that described in our previous article [23]. Briefly, the photolysis was effected by an excimer laser (Lambda Physik, Model Compex-102, Fluorine version), and the product OH was probed by a Quantel dye laser, with frequency doubling and the mixing module (TDL 90), pumped by a Quantel seeded Nd:YAG laser (model YG 980 E-20). The reaction chamber was made of glass with crossed arms at right angles, provided for the entrance of the pump and the probe laser beams, which intersect at the center of the reaction chamber. The detection system was attached to the bottom window, to capture a view of the intersection volume of the photolysis and the probe lasers. This system consisted of a lens (focal length 50 mm, diameter 38 mm) to collect the fluorescence, a photomultiplier tube (Hamamatsu, model R 928P) to detect it, and a band pass filter (λ_{centre} = 310 nm, FWHM = 10 nm, $\%T_{310nm}$ = 10%) placed between them to cut off the scattering from the photolysis laser light. The fluorescence signal was gate integrated by a boxcar (SRS 20), averaged over 30 laser shots, and fed into an interface (SRS 245), for A/D conversion. The dye laser output was scanned by a PC via an RS232 interface, and the same was used to collect the data through a GPIB interface, using a control and data acquisition program. LIF intensities were normalized with respect to both the pump and the probe laser energies, using suitable photodiodes, to correct for the laser intensity fluctuations.

The vapour of the compound (at a pressure of ~10 mTorr) was flowed through the reaction chamber at a flow velocity of approximately 10 cm/s, and was photolysed by ArF laser at 193 nm. The OH fragment was probed state selectively by exciting the $A^2\Sigma \longleftarrow X^2\Pi$ (0,0) transition of OH (306–309 nm), and monitoring the subsequent $A \rightarrow X$ fluorescence. Both the laser beams were unfocussed and attenuated, to prevent any saturation effect or multiphoton event. LIF signal was found to be linearly proportional to the laser powers. The linearity of the LIF signal also ruled out any interference from TFA dimer, which, anyway is unlikely to form under such low pressure and high flow velocity.

Absorption cross section of TFA was measured by filling a known pressure of the sample into a 50 cm long cylindrical absorption cell, fitted with MgF_2 windows at both ends, and placing it in the excimer laser beam. TFA is known to form dimer at room temperature, hence, pressure was kept very low (between 2–5 torr) to minimize dimer formation. Sample pressure in the cell was measured with a capacitance manometer. A beam splitter was placed in front of the cell for dividing the original laser beam into two parts, one for passing through the sample and the other as a reference. Two photodiodes were used for measuring the intensities of the sample beam, after exit from the sample cell and the reference beam. By measuring ratio of the intensities of the two beams, fraction of the intensity absorbed by the sample was determined. This fraction was plotted against the number of molecules in the cell in a semilog plot. Within the experimental range of pressures, the relation was found to be linear, thus overruling any significant contribution of dimers. Using Lambert-Beer's law, absorption cross section of TFA molecule at 193 nm was calculated. This value was used for determination of the quantum yield of the OH formation channel from TFA on excitation at 193 nm.

A stainless steel cell, with crossed arms at right angles to each other, and fitted with suitable windows, for allowing UV and IR light, was used for both Gas Chromatography–Mass Spectrometry (GC—MS), infrared fluorescence (IRF) and FTIR studies. The cell was filled with TFA (around 1 Torr) and photolysed by about 1000 pulses of 193 nm laser with the average pulse energy of about 4–5 mJ, and the IRF was collected and measured at discrete wavelengths, using appropriate band pass filters. The emission was detected at right angle geometry by a liquid N_2 cooled InSb detector (IS-2.00 Graseby), equipped with a matched pre-amplifier. The output signal was fed to a Lecroy (9350 A) digital oscilloscope, for digitization, averaging and background subtraction. The same irradiated sample was used for recording the FTIR absorption spectrum by a Bruker IFS 66v/S FTIR instrument, and the stable products were analyzed qualitatively by separating with Q-plot column, employing GC—MS (Chemito GC 8610).

2.2. Theoretical calculations

To understand the complete implications of the experimental results, theoretical calculations were done using Gaussian 03 suite of programmes [24]. To compare the dissociation energy of C—OH bond from the for AA, DFA and TFA, the ground state structure of these three molecules and the products C—OH bond breaking were optimized at MP2/6-311 + + G** level. The energies of the optimised structures were also calculated at the same level and the C—OH bond dissociation energy ($D_0 = h\nu - E_{avl}$) were determined.

To gain complete information about the overall dissociation process of TFA, we evaluated its ground state dissociation channels theoretically at MP2/6-311 + + G** level of theory. All the relevant stationary structures and transition states were geometry optimized and their energies were calculated at the same level.

The equilibrium geometry of the lower excited electronic states (S_1 and T_1) was optimised at the CIS/aug-cc-pvdz level and these geometries as well as energies were used for obtaining the vertical excitation energies for various transitions. The nature of the orbitals involved in the transition effected by absorption at 193 nm was obtained at this level. To find the nature of the lower energy excited states, potential energy curves for the ground state (S_0) and the first singlet and triplet (S_1 and T_1) of TFA was mapped at the time-dependent B3LYP/6-311 + + G** level as a function of the C—OH bond length. The geometry was frozen to the equilibrium position of the respective states except for variation in the C—OH bond length.

Results of these theoretical calculations are discussed in the relevant sections.

3. Results

3.1. Detection of OH on excitation of TFA at 193 nm

The UV photolysis of TFA at 193 nm leads to formation of OH radical as a transient radical product which was detected by its LIF signal. The state selective distribution of the nascent OH radicals was probed by measuring fluorescence of the A-X(0,0) system, after exciting the same system with frequency doubled tunable dye laser. Similarly, an attempt was made to measure the product OH ($v'' = 1, J''$) by exciting the A-X(1,1) transition, but no detectable signal was observed. Thus, OH formed in higher vibrational levels ($v'' > 0$) is negligible, i.e., the OH generated was found to be vibrationally cold. Several rotational lines were measured (shown in Fig. 1), to obtain information about the OH formation dynamics.

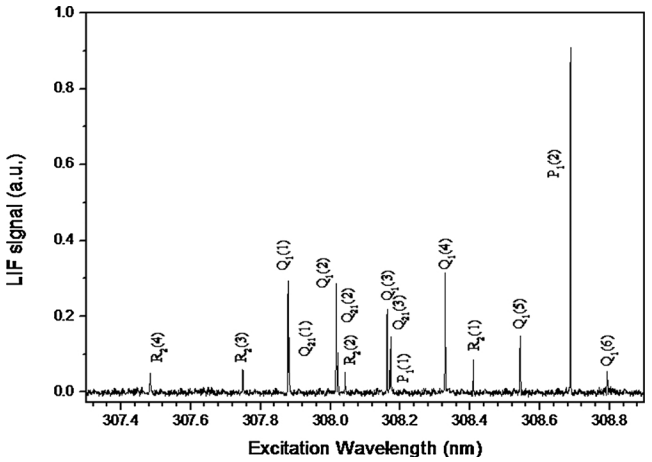

Fig. 1. A portion of the fluorescence excitation spectrum of the (0, 0) band of the $A^2\Sigma \longleftarrow X^2\Pi$ (0,0) system of OH, generated in photodissociation of TFA at 193 nm. The pressure of TFA was maintained at around 10 mTorr, and pump-probe delay was kept at around 50 ns.

3.1.1. Rotational temperature

The positions of all the rotational lines in the spectrum of the OH radical were marked following the assignments made by Dieke and Crosswhite [25]. The respective LIF intensities were normalized with respect to photolysis and the probe laser intensities, pressure of the sample in the cell, and Einstein's absorption coefficients B_{ij} [26], to calculate the relative population of each rotational level.

The normalized populations P(J") of the nascent OH fragment were plotted against energy of rotational levels (ε), to construct a Boltzmann plot given by the equation,

$$ln\,\frac{P(J")}{(2J"+1)} = \frac{-\varepsilon hc}{kT_R} + constant \tag{1}$$

From the slope of this plot (depicted in Fig. 2), rotational temperature (T_R) of OH in the vibrational ground state was found to be (410 ± 40)ºK, which corresponds to (0.8 ± 0.1) kcal/mol.

3.1.2. Spin-orbit and Λ doublet state distribution

The ratios of the populations of $^2\Pi_{3/2}$ and $^2\Pi_{1/2}$ states, multiplied by appropriate statistical weights (2J"+1), were plotted against respective rotational quantum numbers (N).

The plot (given in Fig. 3) shows the ratio is close to unity, for all values of N. Hence, it can be concluded that the distribution of OH

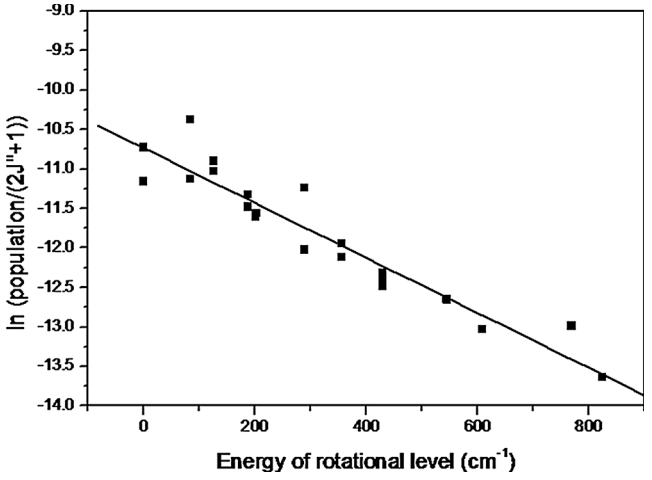

Fig. 2. Boltzmann plot of rotational state population against the energy of rotational states of OH (v″ = 0) generated in dissociation of TFA at 193 nm.

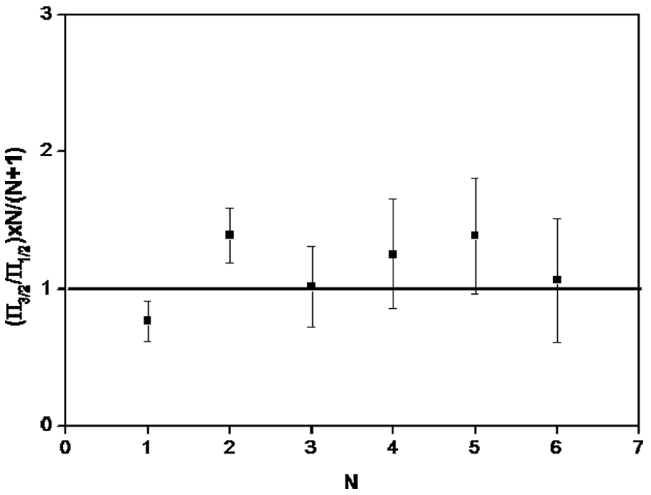

Fig. 3. Distribution of the ratio of spin-orbit state populations against rotational quantum number N for the OH radical produced in photodissociation of TFA at 193 nm.

population between these two states is statistical, and there is no preference for either of these spin-orbit states. The statistical distribution of the population generally implies that the dissociating state is probably not a triplet state, which could have given a preferential distribution in a particular spin-orbit state. In photodissociation of DFA [16], a preference towards $^2\Pi_{1/2}$ state was reported.

But, statistical distributions of the spin-orbit states of OH, generated by photolysis of TFA [14], AA [16], propiolic acid [27] and pyruvic acid [28], at 193 nm, are reported, though the dissociating state is the lowest triplet state in all of them. The difference in the orientation of π lobes with respect to the plane of rotation of the molecule gives rise to Λ doublets. In $^2\Pi^+(A')$ states of OH, the π lobe lies in the plane of rotation while in $^2\Pi^-(A'')$ state, the π lobe lies perpendicular to the plane of rotation. The populations of $^2\Pi^+(A')$ and $^2\Pi^-(A'')$ states were measured from P and Q lines, respectively. From the ratio of populations of these two states (shown in Fig. 4), it is evident that the two levels are roughly equally populated, particularly at higher rotational states. Similar result was also obtained earlier by Kwon et al. [14]. From our results, as well as that of Kwon's, it can be inferred that both impulse and parent torsion should transform in product rotational motion.

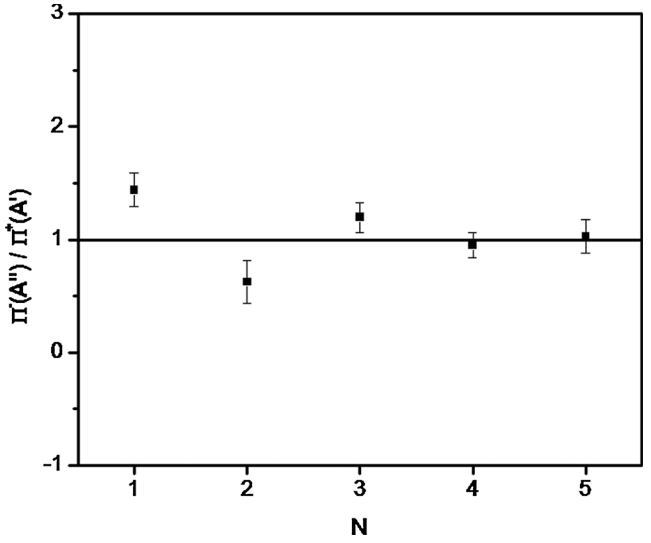

Fig. 4. Dependence of ratio of Λ-doublet populations on rotational quantum number *N* for the nascent OH formed in laser induced photodissociation of TFA at 193 nm.

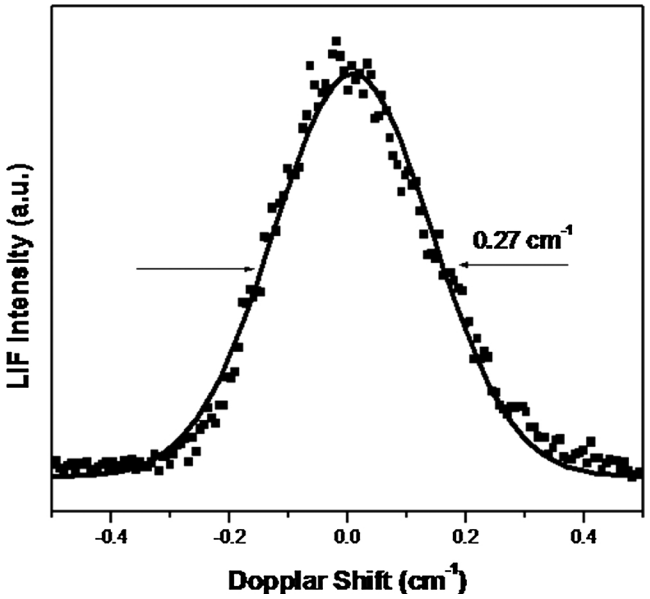

Fig. 5. Doppler-broadened $P_1(2)$ line of the $A^2\Sigma \longleftarrow X^2\Pi$ (0,0) system of the OH radical, produced in dissociation of TFA at 193 nm.

3.1.3. Translational energy in products

Translational energy partitioned in the products was obtained from the Doppler-broadened rotational lines. A typical measured Doppler profile of the $P_1(2)$ rotational line is depicted in Fig. 5.

The Doppler-broadened LIF lines have contributions from different line broadening factors, like molecular velocity of the fragments, thermal motion of the parent molecule, and the finite probe laser width. Hence, after correcting for the probe laser line width (0.07 cm^{-1}), the Doppler profile of a line in the spectrum shows the distribution of velocity component v_z of the absorbing species, i.e. the OH radical along the propagation direction of the probe laser beam. This velocity component v_z is related to the linear Doppler shift $\Delta\nu_D$ through the equation

$$\Delta\nu_D = \nu - \nu_0 = \frac{v_z \nu_0}{c} \tag{2}$$

where v_0 is the central frequency of the rotational line. If the velocity distribution f(v) is isotropic, i.e., $f(v_x) = f(v_y) = f(v_z)$, then the average translational energy, in the laboratory frame, is given by,

$$E_T^{lab}(\mathrm{OH}) = \frac{3}{2} m_{\mathrm{OH}} < v_z^2 >_{\mathrm{OH}} \tag{3}$$

where, $< v_z^2 >_{OH}$ is given by Eq. (4) for a Gaussian Doppler profile as,

$$<v_z^2>_{\mathrm{OH}} = \frac{(FWHM/2\nu_0)^2 c^2}{2\,ln\,2} \tag{4}$$

where, FWHM is the width of the Doppler profile. The widths of the $P_1(2)$ line were measured, and using the above two equations, the kinetic energy of the OH fragment in laboratory frame, $E_T^{lab}(OH)$, was determined. The average translational energy in the centre of mass frame, E_{CM}, was calculated from $E_T^{lab}(OH)$, neglecting the translational energy of the parent molecule, by the use of the equation,

$$E_T^{CM} = E_T^{lab}(\mathrm{OH}) \left[1 + \frac{m_{\mathrm{OH}}}{m_{otherfragment}} \right] \tag{5}$$

and found to be 10.2 ± 1.0 kcal/mol.

3.2. Quantum yield measurement for formation of OH from photolysis of trifluoroacetic acid at 193 nm

Using Lambert-Beer's law, absorption cross section of TFA molecule at 193 nm was calculated to be 7.17×10^{-20} cm^2 $molecule^{-1}$. The yield of the OH radical is directly proportional to the absorption cross section(σ) of the parent molecule at 193 nm. All the measurements were performed at high pressure and longer delay time, which were sufficient enough to thermalize the OH radicals produced. Hence, the intensity of an OH rotational line, normalized for the absorption cross section(σ) of the parent molecule, gives information on quantum yield of its generation channel. We calculated the quantum yield of OH generation from TFA by relative method, using the relation

$$\frac{Q.\,Y_{\cdot sample}}{Q.\,Y_{\cdot reference}} = \frac{\left(\frac{intensity}{\sigma}\right)_{sample}}{\left(\frac{intensity}{\sigma}\right)_{reference}} \tag{6}$$

Acetic acid was taken as the reference compound with the measured values of the absorption cross section and quantum yield of OH generation channel to be 1.13×10^{-19} cm^2 $molecule^{-1}$ and 0.8, respectively[18]. The areas under the curve of $P_1(2)$ line of TFA and AA were compared, and the quantum yield of OH formation channel from TFA was determined to be about 0.4, almost half of the OH quantum yield of AA.

3.3. Analysis of the stable products of photolysis of trifluoroacetic acid at 193 nm

The stable products of the photolysis of TFA were analysed, using FTIR and GC–MS technique. A number of peaks could be detected, in the FTIR absorption spectrum (Fig. 6) of the resultant mixture, after photolysing TFA by 193 nm laser. The peaks are assigned to possible products, following assignments made by Jollie et al. [11], and Pacansky et al. [29] (Table1). The products identified are CHF_3, C_2F_4, CF_3COF, HFPO, CF_2O, CO and CO_2. Among these, CO_2, C_2F_4, and CHF_3 were also confirmed by the GC–MS method.

3.4. Detection of vibrationally excited products of photolysis of TFA

Infrared fluorescence of the irradiated sample was collected at discrete wavelengths, using appropriate band pass IR filters. Fluorescence was detected at 4.3 μm and 4.7 μm, and attributed to vibrationally excited CO_2 and CO, respectively. The formation of these vibrationally excited products has also been detected earlier in the IRMPD of TFA [12].

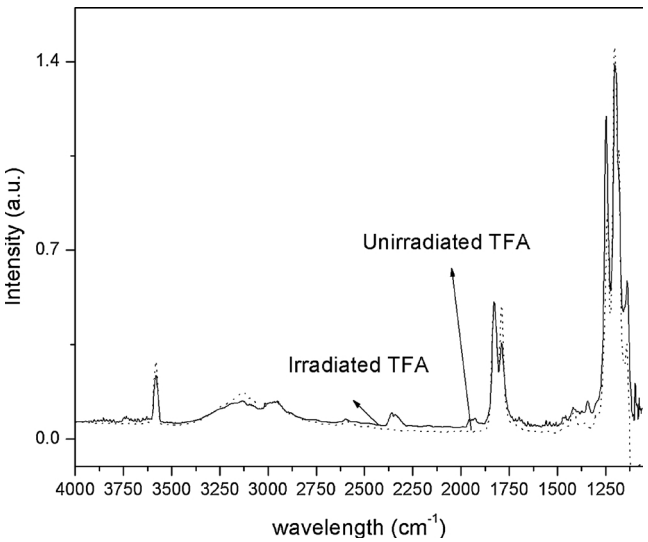

Fig. 6. FTIR spectra of TFA, before and after laser irradiation at 193 nm. The peaks are assigned to the individual stable products in (Table 1).

Table 1
The detection of different stable products of dissociation of TFA by 193 nm laser by the peaks obtained in the FTIR spectrum of the irradiated sample. Peaks are assigned following the reports by Jollie et al. [11] and Pacansky et al. [29].

Observed peak	species	Reference peak
1085	CF_3COF	1092 [11]
1097	CF_3COF	1100 [11]
1106	CF_3COF	1107 [11]
1128	HFPO	1128 [11]
1153	CHF_3	1152 [11]
1192,1195	TFA(parent)	
1203	CF_3COF	1207 [11]
1247	HFPO	1235 [11]
1282	HFPO, CF_4	1282 [11]
1340	C_2F_4	1338 [11]
1375	HFPO	1375 [11]
1419	$(CHF_2)_2O$	1419 [11]
1560	HFPO	1560 [11]
1943	CF_2O	1943 [11]
1957	CF_2O	1957 [29]
2103–2208	CO	2141 [11]
2281–2381	CO_2	2234–2396 [11]
3045	CHF_3	3035 [11]

4. Results and discussion

As we studied the photodissociation dynamics of TFA, and compared with previous studies on AA and DFA, we found that the distribution of available energy in different degrees of freedom is very similar, and hence the reaction pathway must also be quite similar. However, the quantum yield of OH formation was found to be much lower in TFA (0.4) compared to AA (0.8). Kwon et al. also has reported the similarity between the reaction mechanism of OH formation by photolysis of TFA and AA at 193 nm [14], and attributed the major dissociation channel to be from T_1 state which is populated by adiabatic ISC from the optically excited S_1 state. But, currently, detailed theoretical studies done at advanced level of theory suggested that in case of trifluoroacetic acid and acetic acid, direct dissociation from the S_1 state is probably a major reaction channel. To understand the mechanism for formation of transient OH radical and the observed stable products from TFA in our experiment, we performed theoretical study, using Gaussian 03 suite of programmes [29]. We compared our experimental and theoretical results with the earlier theoretical calculations on AA [17] and DFA [16].

4.1. Bond dissociation energy: dynamics of OH generation chanel

The C—OH bond dissociation energy ($D_0 = h\nu - E_{avl}$) in ground state of different fluorinated alcohols has been calculated theoretically using different levels of theory and compared with acetic acid(AA). Kwon et al. calculated the dissociation energies (D_0) of AA and TFA to be 110 and 112 kcal/mol using MP2/6-311 + G level of theory [14]. Naik et al. [16] calculated the dissociation energy of difluoroacetic acid (DFA) at the same level to be 106.2 kcal/mol. Fang et al. calculated the dissociation energies of TFA to be 100.5 kcal/mol using MP2/cc-pvdz level of theory [17]. At PMP4/6-31G* level, the dissociation energies of TFA was calculated to be 106.7 kcal/mol by Francisco [21]. Luo et al. calculated the dissociation energy of TFA to be 104.1 kcal/mol, using the complete active space self-consistent field (CASSCF) method [22]. Though, most of these calculations are competent for predicting the ground state dissociation energy, comparison between the molecules is not very easy because different levels are used. For effective comparison, we calculated their C—OH bond dissociation energies of TFA, DFA and AA, at MP2/6-311 + +G** level, by optimizing the ground state equilibrium structures of the parent molecules as well as the dissociation products in the same level. The results showed that the values of bond dissociation energy for TFA, DFA and AA are very close, at 109.1, 108.6 and 108.4 kcal/mol, respectively. The lengths of the C—OH bond are also almost similar in the equilibrium structure of TFA, DFA and AA, at 1.33 Å, 1.34 Å, and 1.35 Å respectively for (Fig. 7).This indicates that the fluorine substitution in the side chain (β-carbon) has negligible influence on the strength of the C—OH bonds in the ground state.

Taking the bond dissociation energy as 109.1 kcal/mol, the available energy for the photodissociation of TFA was found to be 37.9 kcal/mol. The experimentally obtained energy partitioned to the relative translation of the photoproducts (*f(T)*), consists ~26% of the available energy *f(T)*. This value is lower than the *f(T)* suggested by Kwon et al. (33%) [14].

Generally, two different limiting models of dynamics are applied to model the nature of potential energy surface along the dissociation channel. The impulsive model [30] is applicable in the case of dissociation from a repulsive surface, and the statistical model [32] is applicable in the case of barrierless dissociation. In case of OH formation channel from TFA, the Impulsive model predicts an *f(T)* value of ~47%, which is much higher than the experimental value. The Statistical model [31] calculates an *f(T)* value of ~15%, which is much lower. As the experimental *f(T)* value did not match any of the limiting models, we tried Barrier Impulsive Model [31] (Table 2), which is valid

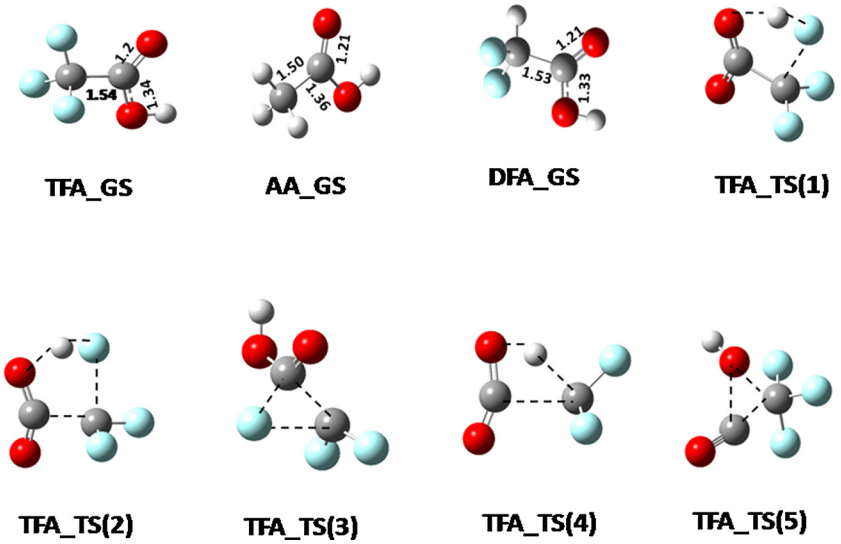

Fig. 7. Ground state structures of TFA, DFA and AA, (TFA_GS, AA_GS, DFA_GS,) optimized at the MP2/6- 311 + +G** level of theory. The important transition states (TFA_TSs), for photodissociation of TFA at 193 nm are also geometry optimized at the MP2/6-311 + +G** level of theory. Details are given in the text.

Table 2
The comparison between the energy distribution among the different modes of photoproducts of TFA for dissociation by 193 nm laser.

	E_T(CM) (kcal/mol)	E_R(OH) (kcal/mol)	f_T	f_R(OH)
CH_3COOH				
Experimental	10.2	0.8	26.0%	2.1%
Impulsive			47.0%	2.3%
Statistical			15.0%	8.7%
Barrier impulsive model (Barrier height ~13 kcal/mol)	9.9	4.0	26.0%	8.0%

when an exit barrier is present in the dissociation channel.

In this model, the exit channel is assumed to have an energy barrier and the total available energy is considered to be divided in two energy reservoirs. The energy released by barrier is considered to be the impulsive reservoir, and the available energy above the height of the exit barrier is considered to be the statistical reservoir. The barrier height is adjusted so that total energy in each degree of freedom of the product matches the experimental values as closely as possible. The barrier height for formation of OH from photodisociation of TFA at 193 nm, as calculated from barrier impulsive model, was found to be ~13 kcal/mol. The presence of an exit barrier is common for mechanisms involving dissociation from an excited state, since a simple bond cleavage in the ground electronic state does not have a barrier. However, if the reaction involves a radical intermediate, it is possible to have a barrier in the ground state electronic state [22,33,34]. Very similar results were observed for the OH formation at photodissociation of AA [18–20] and DFA [16], where the dynamics indicated the presence of exit barrier of similar value in the potential energy surface.

4.2. OH formation channels from excited and ground states

Theoretical calculations on TFA have been carried out to understand the nature of transition involved at 193 nm, and find out the energetically feasible pathways for OH formation from the ground and the electronic excited states. These calculations on AA are performed for a comparison with TFA. The four bands in the 250–140 nm region of the absorption spectra of AA and TFA are assigned as, n-π*, n-3s Rydberg, π-π*, and n-3p Rydberg transitions respectively [35,36]. Absorption at 193 nm, excites the HOMO-LUMO transition in the TFA molecule, the HOMO having $n_{C=O}$ character and the LUMO being the $\pi^*_{C=O}$ orbital. This n-π* transition populates the S_1 excited state of the parent molecule, which is typical of the carboxylic acids including AA [20,37]. Since none of the orbitals involved in this transition, as shown in Fig. 8, has any significant involvement of the side chain, substitution in this part does not have any observable effect on the nature of transition. The equilibrium geometry of the lower excited electronic states (S_1 and T_1) was optimized at the CIS/aug-cc-pvdz level (TFA_S1/AA_S1 and TFA_T1/AA_T1 in Fig. 7) and these geometries as well as energies were used for obtaining the vertical excitation energies for various transitions. The orbitals involved in the transition effected by absorption at 193 nm were obtained at this level (Fig. 8). To find the nature of these states, potential energy curves for the lower excited electronic states of TFA was mapped at the time-dependent B3LYP/6-311 + + G** level as a function of the C—OH bond length. The geometry was frozen to the equilibrium position of the ground state, except for variation in the C—OH bond length. All these states were found to be bound with respect to the C—OH bond. Same theoretical calculations were also performed for AA, and the potential energy curves of the two molecules are compared in Fig. 9. After initial transition to the S_1 state, the molecule may undergo a number of physical and chemical processes including relaxation to the ground state, crossing over to other nearby excited states, eventually some of these de-exciting to the ground state.

The stationary structures in the ground and lower lying excited states of TFA have been explored theoretically by Luo et al. [22]. In this detailed study, the stationary points in the C − OH and C—C potential energy surfaces are optimized at CASSCF/cc-pvtz level of theory, and their energies were also calculated at MS-CASPT2 or SA-CASSCF level with the same basis set. An active space containing 12 electrons and 9 molecular orbitals were selected for all the CASSCF and CASP2 calculations. Similar calculations were done for acetic acid (AA) by Fang et al., using CASSCF/cc-pvdz level of theory composed of 8 electrons in 7 orbitals [17]. We, in this study, shall compare our experimental results with these theoretical studies in order to understand the relation between the OH formation dynamics in the photodissociation of TFA and AA at 193 nm.

For both AA and TFA, it was found that the equilibrium structure as well as the transition state structure for OH formation in S_1 are very similar. In both these carboxylic acids, the minimum in the S_1 state is characterized by a lengthened C═O bond due to n-π* transition. The TS structures for the C—OH bond dissociation from these excited states have the C—OH bond almost broken, and the other C—O bond shortened close to its value in the ground state equilibrium structure. The barrier for this reaction is around 14–15 kcal/mol for both TFA [22] and AA [17].

The optically excited S_1 state can undergo radiationless pathways like internal conversion to the ground state (S_0) or intersystem crossing to lower energy triplet states like T_1 and T_2. In both AA and TFA, the equilibrium structure in the T_1 state is very similar to the S_1 state. The transition state for C–OH bond breaking from T_1 state is also structurally quite similar to that from S_1 state, both in case of AA [17] and TFA [22]. The calculated barrier height for OH formation, however, from T_1 state for TFA, was found to be around 10 kcal/mol lower than that in AA.

Luo et al. [22], in their high level theoretical calculations, could detect an intersystem crossing (ISC) between the S_1 state and the T_2 state at the FC region in case of TFA, with a high value of the spin-orbit coupling constant. From the T_2 state, the molecule can easily relax to the T_1 state via a conical intersection that exists near the FC region. From the T_1 state, however the C—C bond dissociation is energetically more favourable than the C–OH bond cleavage. Therefore, on excitation of TFA at 193 nm, the C—C bond dissociation from the T_1 state was found to compete effectively with the C–OH bond cleavage from the S_1 state. The height of the exit barrier present in the dissociation channel is expected to be directly responsible for the relative translation of the photoproducts (f_T). The height of the exit barrier in the OH formation channel from S_1 and T_1 channel was calculated to be around 9.5 and 3.8 kcal/mol, respectively, by Luo et al. [22]. The experimentally obtained relative translational energy in this work is 10.2 kcal/mol, which is closer to the barrier height in the S_1 state. Moreover, dissociation from the T_1 state is expected to lead to a non-statistical distribution in the spin-orbit states of the OH radical, which was not observed experimentally either in the present or Kim's work. Therefore, our experimental results are in agreement with the theoretical prediction by Luo et al., that OH formation in the photodissociation of TFA by 193 nm laser proceeds majorly through adiabatic dissociation from the optically excited S_1 state, with some minor contribution from the T_1 state.

In case of AA, too, an S_1 to T_1 intersystem crossing was found near the FC region [17], with high spin orbit coupling. Therefore, non-adiabatic transition from S_1 to T_1 was found to compete with direct dissociation from the S_1 state, albeit the former being unfavoured by spin selection rule. Unlike TFA, in case of AA, the energy requirement for the C–OH bond dissociation in the T_1 state was found to be more favourable than the C—C bond dissociation. Therefore, in case of AA, the excited state C—C bond dissociation is comparatively less significant, and the C–OH bond dissociation from the S_1 or T_1 state seems to be the dominant dissociation channel.

Theoretical results clearly reveal that the overall mechanism for formation of the OH radical by photodissociation of TFA and AA to be very similar. The structures as well as the relative energetic, including

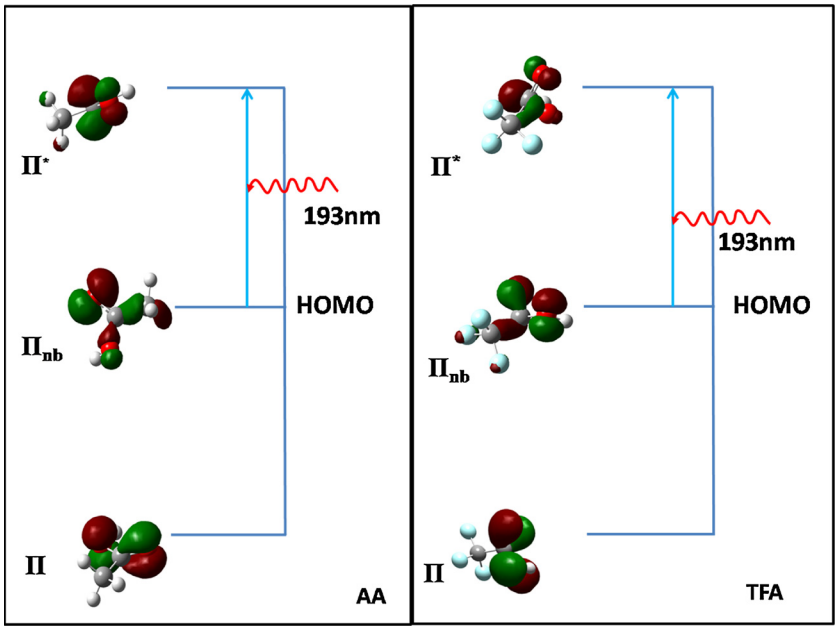

Fig. 8. The π(HOMO-1), π_{nb}(HOMO), and π*(LUMO) orbitals of AA and TFA involved in the lower energy electronic transitions. The n-π* transition to S_1 state populated by absorption at 193 nm is indicated in the figure.

that of the transition states involved in the pathway, were also found to be very similar for these two compounds. This explains the major similarity between the dynamics of OH formation by 193 nm for these two molecules. However, the quantum yield for OH formation was found to be considerably low in case of TFA. The explanation of this must lie in the fact that, in case of AA, OH formation is energetically more favourable than the C—C bond dissociation both from the S_1 and T_1 states. But in case of TFA, OH can majorly be formed from only the S_1 state, as from the T_1 state the C—C bond dissociation is more favourable. Due to this higher extent of competition from the non-adiabatic C—C bond dissociation channel from the T_1 state, the overall quantum yield of the OH radical decreases in case of TFA.

Apart from dissociation directly from the excited states, energized TFA molecule may also de-excite to the ground state and dissociate from there. At the ground state, we optimized all the equilibrium structures relevant to the OH formation at MP2/6-311 + + G** level of theory, and calculated their respective energies in the same level. The ground state optimized structure of TFA, as shown in Fig. 7, is very similar to that of AA, where all C and O atoms lie in the same plane. The double bond is delocalized within the −COOH group, with the C═O bond length as ~1.21 nm and the C–OH bond length as 1.33 nm. This delocalization makes the C—OH bond much stronger than the C—C bond (bond length of ~1.54 nm), in the ground state of TFA. At this level of theory, the C–OH bond dissociation energy of TFA was calculated to be 109.1 kcal/mol, and that of AA to be 109.9 kcal/mol, and no transition state for the OH formation could be detected from either of these molecules. The absence of a TS is expected as simple bond cleavage from the ground state is generally barrierless. These results agree with previous reports on the ground state dissociation of AA [17] and DFA [16]. The similarity in the bond dissociation energy of the barrierless formation of OH from the ground state of TFA and AA can't explain the observed pronounced difference in their quantum yields. Thus, the OH formation from the ground state can be considered a less probable channel for both these compounds. The high endothermicity also makes the direct OH formation from the ground state to be dynamically unfavourable compared to other lower energy channels. Therefore, it can be surmised that OH formation in the photodissociation of TFA by 193 nm laser proceeds mainly through adiabatic dissociation from the optically excited S_1 state.

4.3. Formation of stable products: ground state dissociation channels

In this study, the species unambiguously detected among the stable products of the photolysis of TFA are CHF_3, C_2F_4, C_2F_6, CO_2, CO, CF_3CFO, CF_2O, and hexafluoropropylene oxide (HFPO). All of these products except for C_2F_6 were earlier detected as products of pyrolysis of TFA [11]. CO, CF_3H, and CO_2 are reported as products of thermal decomposition [8], and CO, C_2F_4, C_2F_6, CF_2O and CO_2 are reported to be formed by IRMPD of TFA and its anhydride [12,39]. In the present work, we evaluated the probable ground state dissociation channels of TFA theoretically at MP2/6-311 + + G**level of theory. All the relevant structures were geometry optimized and their energies were calculated at the same level. The calculated values of the activation barriers (ΔE_b) and the energy of the reactions (ΔH_{rxn}) are presented in Table 3 and Fig. 10.

As shown in Table 3, the major reaction channels from the ground state that we have explored can be divided into two major categories, radical channels (producing radical products) and molecular channels (producing molecular products). The energetics of these channels are listed below:

Molecular channels:

$$CF_3COOH \rightarrow HF + F_2CC(—O—)C = O \quad (7)$$

$$CF_3COOH \rightarrow :CF_2 + HF + CO_2 \quad (8)$$

$$CF_3COOH \rightarrow :CF_2 + FCO_2H \quad (9)$$

$$CF_3COOH \rightarrow CF_3H + CO_2 \quad (10)$$

$$CF_3COOH \rightarrow CF_3OH + CO \quad (11)$$

Radical channels:

$$CF_3COOH \rightarrow CF_3 + CO_2H \quad (12)$$

$$CF_3COOH \rightarrow CF_3CO + OH \quad (13)$$

$$CF_3COOH \rightarrow CF_3CO_2 + H \quad (14)$$

For carboxylic acids with hydrocarbon side chain like AA, dehydration or decarboxylaion is reported to be the lowest energy channel [38], whereas for DFA [16], the lowest energy dissociation channel is 1,3 HF elimination through a 5-membered transition state. Francisco

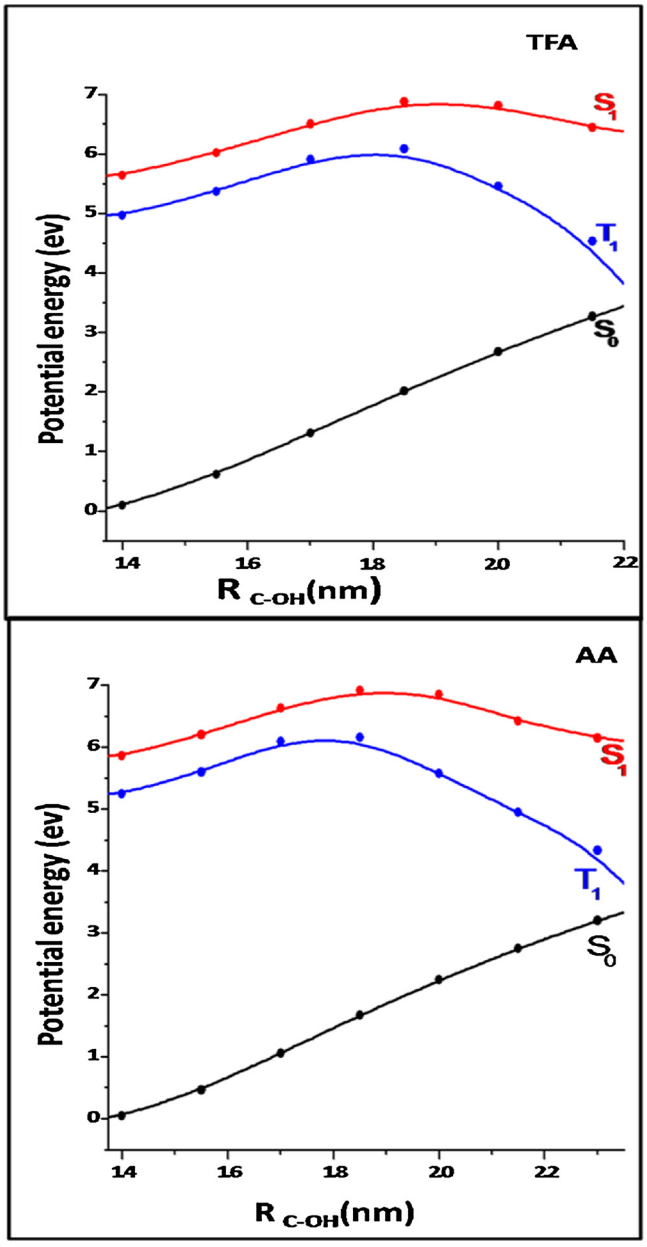

Fig. 9. Potential energy curves for the ground and the lowest singlet and triplet excited electronic states (S_1 and T_1) of TFA and AA calculated with the time-dependent B3LYP/aug-cc-pvdz method as a function of the C—OH bond length. The geometry was frozen to the equilibrium position of the respective states except for variation in the C—OH bond distance. The potential energy of the excited states are calculated by adding the vertical excitation energy to the energy of the respective ground state structure at each point.

[21], however, did not consider HF elimination in his theoretical studies of ground state dissociation channel of TFA, and reported C—C bond dissociation with/without F –atom migration as the lowest energy channels. On the contrary, our theoretical calculations revealed that the HF elimination channel (Reaction (7)), with the activation barrier of ~59.5 kcal/mol, is the lowest energy channels from the ground state. This channel has a five-membered transition state, shown as TFA_TS(1) in Fig. 9. One more low-energy HF elimination channel could also be theoretically optimized, with CO_2 and difluorocarbene $:CF_2$ as co-products. This channel (Reaction (8)), too, has a five-membered transition state TFA_TS(2) in Figs. 9 and 10 lying atop a 62.5 kcal/mol barrier. $:CF_2$ can also form through 1,2 F-atom shift (Reaction (9)), which is proposed as the major $:CF_2$ formation channel in Francisco's report

Table 3
The energetics of different ground state reaction channel for the photodissociation of TFA at 193 nm. Energy calculations were done at the MP2/6-311 + + G** level of theory, on geometries optimized at the same level.

Reaction Channel		Energy (kcal/mol)
Molecular channels		
$CF_3COOH \rightarrow HF + F_2CC(O)O$	ΔE_b	59.5
	ΔH_{rxn}	40.9
$CF_3COOH \rightarrow :CF_2 + CO_2 + HF$	ΔE_b	64.2
	ΔH_{rxn}	39.1
$CF_3COOH \rightarrow :CF_2 + FCO_2H$	ΔE_b	80.3
	ΔH_{rxn}	10.6
$CF_3COOH \rightarrow CF_3H + CO_2$	ΔE_b	76.5
	ΔH_{rxn}	−19.2
$CF_3COOH \rightarrow CF_3OH + CO$	ΔE_b	107.9
	ΔH_{rxn}	2.3
Radical channels		
$CF_3COOH \rightarrow CF_3 + CO_2H$	ΔH_{rxn}	91.7
$CF_3COOH \rightarrow CF3CO_2 + H$	ΔH_{rxn}	112.7
$CF_3COOH \rightarrow CF3CO + OH$	ΔH_{rxn}	109.1

[21]. We, however, expect this channel to be less favourable than Reaction (8), as it has a much higher energy barrier (80.3 kcal/mol), due to involvement of a high energy 3-membered transition state (TFA_TS3 in Fig. 7). The presence of $:CF_2$, however, could only be inferred by detection of the secondary products of its reactions. The formation of CF_3H, C_2F_4, CF_2O and HFPO (hexafluoropropylene oxide), all detected as stable products, could be attributed to the following reactions of $:CF_2$ [11]:

$$HF + :CF_2 \rightarrow CF_3H \quad (15)$$

$$CF_2 + CO_2 \rightarrow CF_2O + CO \quad (16)$$

$$CF_3COF + :CF_2 \rightarrow \quad CF_3FC\!-\!CF_2 \ (\text{HFPO}) \quad (17)$$

$$CF_2 + :CF_2 \rightarrow C_2F_4 \quad (18)$$

HF and its co-products could be detected in a number of studies [11]. The formation of CF_3COF (detected in FTIR), can be considered a secondary product formed by the reaction of HF with the parent molecule:

$$HF + CF_3CO_2H \rightarrow CF_3COF + H_2O \quad (19)$$

Another low energy channel that we could optimize is the formation of CF_3H and CO_2 through C—C bond breaking and simultaneous 1,3 H-atom shift (Reaction (10)). We could optimize the 4-membered transition state of this rearrangement channel, which lies atop an activation barrier of 76.5 kcal/mol (TFA_TS(4) in Figs. 9 and 10). This channel was found to have an exoergicity of about 15.48 kcal/mol, that can be distributed as the internal energy of the products. This leads to the formation of CO_2 in vibrationally excited state, as detected by its IR fluorescence. C—C bond breaking may also take place simultaneously with 1,2 shift of the −OH group (Reaction (11)). This channel has been proposed by Osborne et al. as one of the major channels for CO formation [15]. But this channel involves a strained 3- membered transition state (TFA_TS(5) in Figs. 9 and 10), and demands high activation energy (107.9) kcal/mol). Hence it is not expected to be a major channel.

The direct C—C bond breaking (Reaction (12)) in TFA has an endothermicity of 91.7 kcal/mol. It is important to note that though it may not be the lowest energy channel, it must be one of the major channels of dissociation as experimental evidence for formation of a good yield of CF_3 was found in the detection of its dimer, C_2F_6.

$$CF_3 + CF_3 \rightarrow C_2F_6 \quad (20)$$

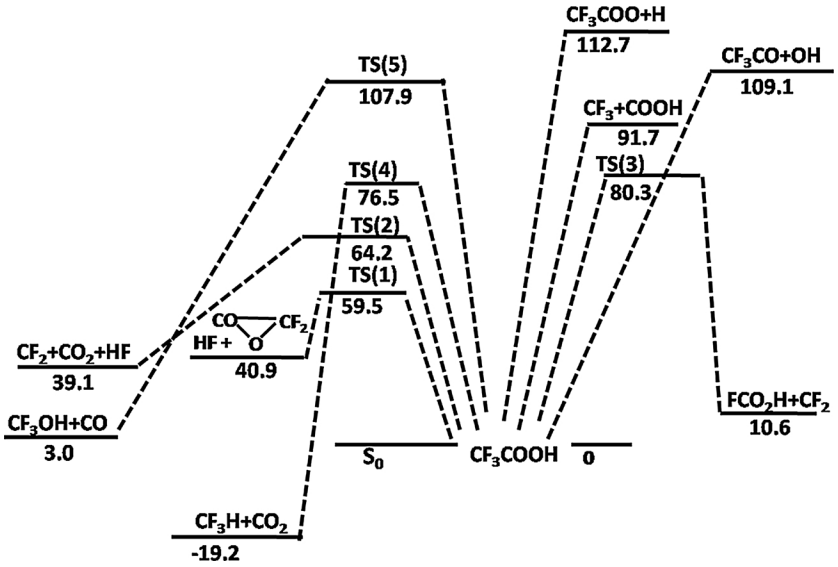

Fig. 10. Potential energy diagrams for the dissociation channels from the ground state of TFA. Equilibrium structures are optimised and energies are calculated at the MP2/6-311 + + G** level. All energies are in kcal/ mol.

Direct OH radical formation from ground state through C–O bond breaking Reaction (13) has been found to be very high energy channel both by Francisco [21] and the present work (109.1 kcal/mol). This dissociation channel should have negligible quantum yield from the ground state, as it is more energy demanding than most of the other available channels, except for direct O—H bond breaking (Reaction (14)), which has a reaction enthalpy of 112.7 kcal/mol.

Overall, our theoretical calculations show that the relative energetics of the ground state dissociation channel of TFA is similar to the other fluorinated carboxylic acids like DFA and different from AA.

5. Conclusion

Our experimental and theoretical studies explored the photodissociation channels from the ground and the excited state for of trifluoroacetic acid (TFA) at 193 nm, as a representative of the fluorinated carboxylic acids. The results were compared with the previous reports of photodissociation of acetic acid (AA) and difluoroacetic acid (DFA), to understand how replacement of hydrogen by fluorine on the α-C atom changes the mechanism of the dissociation reaction. The dynamics of OH elimination channel was found to be similar in the case of all the three molecules, indicating fluorination at the α-C atom of carboxylic acids does not significantly change the mechanism of the C—OH bond scission. In all the cases, the major OH formation channel is from the S_1 state, with an exit barrier, with some contribution from T_1 state. Though the dynamics for OH formation was found to be similar for TFA and AA, the quantum yield in case of the former was found to be much higher. This could be attributed to the fact that in case of AA, C–OH bond breaking was energetically favourable from both S_1 and T_1 state. But in case of TFA, C—C bond breaking is more favourable in the T_1 state. Some fraction of the excited molecules relaxes back to the ground state, and undergoes different dissociation channels, to generate various stable products as detected by GC and FTIR. Theoretical calculations revealed that in all the three molecules, C—OH bond cleavage from the ground state is a high energy channel. However, it was found that though in AA, decarboxylation and dehydration are lowest energy channels from ground state, in case of its fluorinated analogues, TFA and DFA, HF elimination requires the lowest energy. Thus, we could conclude that though fluorination at the C atom in the side-chain of aliphatic carboxylic acids does not significantly change the potential energy surfaces of the C—OH bond scission, it considerably alters the relative energetics of the ground state dissociation channels.

Conflict of interest

The authors declare no conflict of interest.

Acknowledgments

The authors are grateful to Ms. Asmita Sharma of RPCD, BARC for helping in carrying out the GC–MS experiments. The authors are also indebted to their colleague, Dr. H. P. Upadhyaya, for his valuable inputs.

References

[1] C.A. Guy, G.B. Fields, Trifluoroacetic acid cleavage and deprotection of resin-bound peptides following synthesis by Fmoc chemistry, Methods Enzymol. 289 (1997) 67–83.
[2] S.J. Stou, A.R. DaCunha, Tuning and calibration in thermospray liquid chromatography/mass spectrometry using trifluoroacetic acid cluster ions, Anal. Chem. 61 (1989) 2126–2128.
[3] T.J. Wallington, W.F. Schneider, D.R. Worsnop, O.J. Nielsen, J. Sehested, W.J. Debruyn, J.A. Shorter, The environmental impact of CFC replacements HFCs and HCFCs, Environ. Sci. Technol. 28 (1994) A320–A326.
[4] D.A. Ellis, J.W. Martin, A.O. De Silva, S.A. Mabury, M.D. Hurley, M.P.S. Andersen, T.J. Wallington, Degradation of fluorotelomer alcohols: a likely atmospheric source of perfluorinated carboxylic acids, Environ. Sci. Technol. 38 (2004) 3316–3321.
[5] D.J. Bowden, S.L. Clegg, P. Brimblecombe, The Henry's law constant of trifluoroacetic acid and its partitioning into liquid water in the atmosphere, Chemosphere 32 (1996) 405–420.
[6] L.D. Gruenke, K. Konopka, D.R. Koop, L.A. Waskell, Characterization of halothane oxidation by hepatic microsomes and purified cytochromes P-450 using a gas chromatographic mass spectrometric assay, J. Pharm. Exp. Ther. 246 (1988) 454–459.
[7] M.P.S. Andersen, O.J. Nielsen, B. Karpichev, T.J. Wallington, S.P. Sander, Atmospheric chemistry of isoflurane, desflurane, and sevoflurane: kinetics and mechanisms of reactions with chlorine atoms and OH radicals and global warming potentials, J. Phys. Chem. A 116 (2012) 5806–5820.
[8] A. Ashworth, P.G. Harrison, Fourier-transform infrared study of the gas-phase thermolysis of trifluoroacetic acid, J. Chem. Soc. Faraday Trans. 89 (1993) 2409–2412.
[9] P.G. Blake, H. Pritchard, A.D. Tomlinson, Kinetics and mechanism of the thermal decomposition of difluoroacetic acid, J. Chem. Soc. B (1971) 607–610.
[10] P.G. Blake, H. Pritchard, The thermal decomposition of trifluoroacetic acid, J. Chem. Soc. B (1967) 282–286.
[11] D.M. Jollie, P.G. Harrison, An in situ IR study of the thermal decomposition of trifluoroacetic acid, J. Chem. Soc. Perkins Trans. 2 (1997) 1571–1576.
[12] A. Kumar, R.K. Vatsa, P.D. Naik, K.V.S.R. Rao, J.P. Mittal, Infrared fluorescence from nascent CO_2 and COF_2 photoproducts in IR multiphoton dissociation of trifluoroacetic acid, Chem. Phys. Lett. 208 (1993) 385–391.
[13] A.M. Mearns, R.A. Back, The photolysis of trifluoroacetic acid vapor, Can. J. Chem. 41 (1963) 1197–1206.
[14] H.T. Kwon, S.K. Shin, S.K. Kim, H.L. Kim, C.R. Park, Photodissociation dynamics of

acetic acid and trifluoroacetic acid at 193 nm, J. Phys. Chem. A 105 (2001) 6775–6779.
[15] M.C. Osborne, Q. Li, I.W.M. Smith, Products of the ultraviolet photodissociation of trifluoroacetic acid and acrylic acid, Phys. Chem. Chem. Phys. 1 (1999) 1447–1454.
[16] A. Kumar, H.P. Upadhyaya, P.D. Naik, Dissociation dynamics of difluoroacetic acid from the ground and excited electronic states, J. Phys. Chem. A 108 (2004) 6257–6264.
[17] W.-H. Fang, R.-Z. Liu, X. Zheng, D.L. Philips, Photodissociation of acetic acid in the gas phase: an ab initio study, J. Org. Chem. 67 (2002) 8407–8415.
[18] P.D. Naik, H.P. Upadhyaya, A. Kumar, A.V. Sapre, J.P. Mittal, Dynamics of acetic acid dissociation at 193.3 nm: selectivity in OH reaction channel, Chem. Phys. Lett. 340 (2001) 116–122.
[19] S.S. Hunnicutt, L.D. Waits, J.A. Guest, Energetic constraints in the 218 nm photolysis of acetic acid, J. Phys. Chem. 93 (1989) 5188–5195.
[20] S.S. Hunnicutt, L.D. Waits, J.A. Guest, $^{1}(n,\pi^{*})$ photochemistry of acetic acid at 200 nm: further evidence for an exit channel barrier and reaction selectivity, J. Phys. Chem. 95 (1991) 562–570.
[21] J.S. Francisco, Decomposition pathways for trifluoroacetic acid, CF3C(O)OH, J. Chem. Soc. Faraday Trans. 88 (1992) 3521–3525.
[22] C. Luo, W. Dong, Y. Gu, Theory guided access to efficient photodegradation of the simplest perfluorocarboxylic acid: trifluoroacetic acid, Chemosphere 181 (2017) 26–36.
[23] S. SenGupta, H.P. Upadhyaya, A. Kumar, P.D. Naik, P.N. Bajaj, Detection of OH radical in laser induced photodissociation of tetrahydrofuran at 193 nm, J. Chem. Phys. 122 (2005) 124309-1-7.
[24] M.J. Frisch, G.W. Trucks, H.B. Schlegel, G.E. Scuseria, M.A. Robb, J.R. Cheeseman, J.A. Montgomery Jr., K.N. Kudin, J.C. Burant, J.M. Millam, S.S. Iyengar, J. Tomasi, V. Barone, B. Mennucci, M. Cossi, G. Scalmani, N. Rega, G.A. Petersson, H. Nakatsuji, M. Hada, M. Ehara, K. Toyota, R. Fukuda, J. Hasegawa, M. Ishida, T. Nakajima, Y. Honda, O. Kitao, H. Nakai, M. Klene, X. Li, J.E. Knox, H.P. Hratchian, J.B. Cross, C. Adamo, J. Jaramillo, R. Gomperts, R.E. Stratmann, O. Yazyev, A.J. Austin, R. Cammi, C. Pomelli, J.W. Ochterski, P.Y. Ayala, K. Morokuma, G.A. Voth, P. Salvador, J.J. Dannenberg, V.G. Zakrzewski, S. Dapprich, A.D. Daniels, M.C. Strain, O. Farkas, D.K. Malick, A.D. Rabuck, K. Raghavachari, J.B. Foresman, J.V. Ortiz, Q. Cui, A.G. Baboul, S. Clifford, J. Cioslowski, B.B.G. Stefanov, A.L. Liu, P. Piskorz, I. Komaromi, R.L. Martin, D.J. Fox, T. Keith, M.A. Al-Laham, C.Y. Peng, A. Nanayakkara, M. Challacombe, P.M.W. Gill, B. Johnson, W. Chen, M.W. Wong, C. Gonzalez, J.A. Pople, Gaussian 92, Revision A, 1 ed., Gaussian, Inc., Pittsburgh, PA, 2003.
[25] G.H. Dieke, H.M. Crosswhite, The ultraviolet bands of OH fundamental data, J. Quant. Spectrosc. Radiat. Transf. 2 (1962) 97–199.
[26] I.L. Chidsey, D.R. Crossley, Calculated rotational transition probabilities for the A − X system of OH, J. Quant. Spectrosc. Radiat. Transf. 23 (1980) 187–199.
[27] A. Kumar, H.P. Upadhyaya, P.D. Naik, D.K. Maity, J.P. Mittal, Photodissociation dynamics of propiolic acid at 193 nm: the state distribution of the nascent OH product, J. Phys. Chem. A 106 (2002) 11847–11854.
[28] S. Dhanya, A. Kumar, H.P. Upadhyaya, P.D. Naik, R.D. Saini, Dynamics of OH formation in photodissociation of pyruvic acid at 193 nm, J. Chem. Phys. 118 (2003) 10093–10100.
[29] J. Pacansky, R.J. Waltman, Y. Ellinger, Structures and infrared spectra of perfluoroaldehyde and perfluoroacetaldehyde, J. Phys. Chem. 98 (1994) 4787–4792.
[30] A.F. Tuck, Molecular beam studies of ethyl nitrite photodissociation, J. Chem. Soc. Faraday Trans. 2 (1977) 689–708 73.
[31] J.T. Muckerman, Information theoretic prior functions for large molecular systems, J. Phys. Chem. 93 (1989) 179–184.
[32] S.W. North, D.A. Blank, J.D. Gazelter, C.A. Longfellow, Y.-T. Lee, Evidence for stepwise dissociation dynamics in acetone at 248 and 193 nm, J. Chem. Phys. 102 (1995) 4447–4460.
[33] D.H. Mordaunt, D.L. Osborn, D.M. Neumark, Nonstatistical unimolecular dissociation over a barrier, J. Chem. Phys. 108 (1998) 2448–2457.
[34] D.L. Osborn, H. Choi, D.H. Mordaunt, R.T. Bise, D.M. Neumark, C.M. Rohfling, Fast beam photodissociation spectroscopy and dynamics of the vinoxy radical, J. Chem. Phys. 106 (1997) 3049–3065.
[35] H. Basch, M.B. Robin, N.A. Kuebler, Electronic spectra of isoelectronic amides, acids, and acyl fluorides, J. Chem. Phys. 49 (1968) 5007–5019.
[36] E.E. Barnes, W.T. Simpson, Correlations among electronic transitions for carbonyl and for carboxyl in the vacuum ultraviolet, J. Chem. Phys. 39 (1963) 670–675.
[37] P.D. Naik, H.P. Upadhyaya, A. Kumar, A.V. Sapre, J.P. Mittal, Photodissociation of carboxylic acids: dynamics of OH formation, J. Photochem. Photobiol. C 3 (2003) 165–182.
[38] J.S. Yadav, J.D. Goddard, Acetaldehyde photochemistry: the radical and molecular dissociations, J. Chem. Phys. 84 (1986) 2682–2690.
[39] A. Kumar, R.K. Vatsa, P.D. Naik, K.V.S.R. Rao, J.P. Mittal, Time-resolved infrared fluorescence from an IR multiphoton dissociation product of trifluoroacetic anhydride, Chem. Phys. Lett. 200 (1992) 283–289.